Vortex shedding noise of a cylinder with hairy flaps

Laura Kamps

Technical University Bergakademie Freiberg, Institute for Mechanics and Fluid Dynamics

Thomas F. Geyer, Ennes Sarradj

Brandenburg Technical University Cottbus - Senftenberg, Chair of Technical Acoustics

Christoph Brücker

currently at City University London as Professor at the BAE SYSTEMS Sir Richard Olver Chair in Aeronautical Engineering

Abstract

This study describes the modification of acoustic noise emitted from cylinders in a stationary subsonic flow for a cylinder equipped with flexible hairy flaps at the aft part as a passive way to manipulate the flow and acoustics. The study was motivated by the results from previous water tunnel measurements, which demonstrated that hairy flaps can modify the shedding cycle behind the cylinder and can reduce the wake deficit. In the present study, wind tunnel experiments were conducted on such a modified cylinder and the results were compared to the reference case of a plain cylinder. The acoustic spectrum was measured using two microphones while simultaneously recording the flap motion. To further examine the flow structures in the downstream vicinity of the cylinder, constant temperature anemometry measurements as well as flow visualizations were also performed. The results show that, above a certain Reynolds number, the hairy flaps lead to a jump in the vortex shedding frequency. This phenomenon is similarly observed in the water flow experiments as a jump in the non-dimensional Strouhal number that is related to the change of the shedding cycle. This jump appears to be coupled to a resonant excitation of the flaps and a considerable increase of the flapping amplitude. The specific Reynolds number at which the jump

Email addresses: Laura.Kamps@imfd.tu-freiberg.de (Laura Kamps), Thomas.Geyer@b-tu.de (Thomas F. Geyer)

occurs is higher in the present case, which is attributed to the lower added mass in air as compared with the one in water. The flow visualizations confirmed that such action of the flaps lead to a more slender elongated shape of the time-averaged separation bubble. In addition, the hairy flaps induce a noticeable reduction of the tonal noise as well as broadband noise as long as the flaps do not touch each other.

Keywords: hairy flaps, vortex shedding, flow noise reduction, circular cylinder, wind tunnel

---

1. Introduction

Investigations on sound generated from the flow around cylinders have a long history that goes back to the first observations of aeolian tones [1, 2, 3, 4]. The major mechanism responsible for this sound generation is the intrinsic hydrodynamic instability of the wake downstream from the cylinder that, above a certain Reynolds number, leads to a periodic vortex shedding. As a result, the sound generated from the cylinder is composed of strong tonal components that correspond to the vortex shedding frequency. Additionally, it contains broadband noise due to the turbulent boundary layer that builds around the cylinder. The occurrence of these vortex shedding tones were investigated in detail in 1878 by the physicist Strouhal [5]. Therefore, the non-dimensional shedding frequency was named after him as the Strouhal number

$$St = \frac{f \cdot d}{U_\infty}, \tag{1}$$

where f is the frequency of the vortex shedding tone, d is the cylinder diameter and U_∞ is the free stream velocity.

Due to the practical importance of cylinder wakes in many engineering problems, much attention has been devoted to manipulating vortex shedding with active and/or passive means. Among them, attaching a splitter plate to the cylinder base has been known to be one of the most successful ways of controlling vortex shedding [6]. A known effect of the splitter plate on the wake is a non-monotonically decrease of the shedding frequency with increasing length of the splitter plate. Thereby, the critical length l_c of the plate (non-dimensionalized with the cylinder diameter d) at which the shedding disappears scales linearly with the Reynolds number

$$Re_d = U_\infty d/\nu, \tag{2}$$

with ν being the kinematic viscosity [7]. While several studies considered rigid and undeformable splitter plates for controlling vortex shedding, the effects of the flexibility of a splitter plate have not been studied extensively. Recently, flexible flaps have been investigated by Kunze and Brücker to control the wake generated behind a cylinder. In particular, their device with attached hairy flaps proved that flaps are able to modify the shedding cycle [8]. The study showed a characteristic jump in the shedding frequency at a specific Reynolds number of $Re_{\mathrm{s}} \approx 14{,}000$ when compared to the classical behaviour of a plain cylinder wake flow. The analysis of the motions of the hairy flaps showed that for $Re = Re_{\mathrm{s}}$, the amplitude of the flap motion is considerably increased and a characteristic travelling wave-like motion pattern could be observed along the row of flaps. As a consequence, the presence of the hairy flaps alter the phase within the vortex shedding cycle such that the transversal dislocation (transversal distance from the centerline) of the shed vortices is reduced [8]. Accordingly, the vortices are not arranged in a classical zig-zag pattern of the Kármán vortex-street, but they are rather shed in a row along the centerline. This leads to a noticeable decrease of the length of the separation bubble, which is shown in Figure 1, and a reduction in drag. A main finding from that study was that, if the length of the separation bubble is chosen as the characteristic dimension in Equation (2) instead of the cylinder diameter, the *St*-*Re* plot does not show any jump at all.

Besides a splitter plate, there exists a variety of methods to influence the vortex shedding of circular cylinders and to effectively reduce drag. This includes, for example, different kinds of surface protrusions (like helical strakes, wires, fins or spheres), shrouds and nearwake stabilizers [9], O-rings [10], grooves [11, 12, 13], tripping wire [14] or riblets [15]. However, the novel aspect of the flexible flaps is not only the reduction in drag, but merely the shortening of the separation bubble and, as a consequence, the sudden increase of the Strouhal number associated with the vortex shedding. In future engineering applications such flaps may therefore be used as a means to control the vortex shedding, necessitating of course a comprehensive understanding of their basic operation.

As any modification of the shedding cycle behind the cylinder also has an effect on the generated sound, the objective of the present work is to investigate the acoustics in the flow around cylinders, employing hairy flaps as passive wake-manipulators. In general, solid structures covered with hairs or fibres, such as fluffy bodies, are known to affect the generation of flow

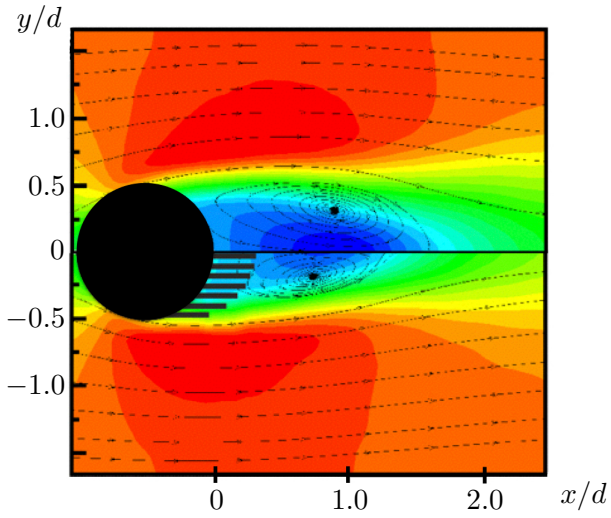

Figure 1: Vortex shedding of a plain cylinder (top) and a cylinder with hairy flaps (bottom) at $Re = 27{,}750$, taken from Particle Image Velocimetry measurements by Kunze and Brücker [8] in a water tunnel (color plot shows contours of constant streamwise velocity)

induced noise [16, 17]. The present investigation intends to describe the consequence of the presence of hairy flaps on the noise generated by cylinders in a flow, especially regarding the spectral modification and possible acoustic damping impact of such flaps.

The remainder of this paper is organized as follows: After this brief introduction and literature review, the experimental setup is described in detail, including the model cylinders, the wind tunnels, the techniques used for the acoustic measurements, the constant temperature measurements and the flow visualization, and the post-processing used for the determination of the flap motion. Further, the results from the different measurements are presented and discussed and finally, conclusions from the present investigation are drawn.

2. Experimental setup

In order to analyze the sound generation by the flow around cylinders with hairy flaps as well as the flap motion, an experimental study was per-

formed on a set of cylinders, which feature modifications that affect the vortex shedding and hence the generation of tonal noise. This study included measurements of the flap motion, acoustic measurements and constant temperature anemometry measurements, which were conducted in the small aeroacoustic wind tunnel at BTU Cottbus - Senftenberg [18]. To obtain additional information on the flow structures in the wake of the cylinder, smoke flow visualization measurements were performed in the wind tunnel at TU Bergakademie Freiberg.

2.1. Wind tunnel

The setup and methodology used for the measurement of the flow noise generated by the cylinders is basically identical to that used in the study by Geyer and Sarradj [19] on the noise generated by porous covered cylinders. It consists of an aerodynamically closed test section of approximately 1.5 m length that is mounted to the rectangular nozzle of the open jet wind tunnel, which has a contraction ratio of about 31.2 and an exit area of 0.23 m $\times$ 0.28 m. The nozzle was specifically built for the purpose of transforming the circular cross section of the wind tunnel to a rectangular cross section at the nozzle exit using the design of Morel [20]. The two lateral sides of the test section are covered by tensioned Kevlar that allows sound waves to propagate from the flow region inside the test section to the outside. The upper and lower walls of the test section are made from thick acrylic glass. Therefore, the test section provides a nearly two-dimensional flow, while at the same time enabling the use of acoustic measurement technique as well as flow visualization technique both of which are positioned outside of the flow region. Figure 2 shows a photograph of this test section. Surrounding the test section is a cabin of dimensions 2.0 m (length) $\times$ 1.5 m (height) $\times$ 1.55 m (width), which has absorbing side walls that lead to a nearly anechoic environment for frequencies above approximately 100 Hz.

With the chosen nozzle, the wind tunnel allows for a maximum flow speed of about 60 m/s. The flow inside the test section can be described as essentially not turbulent, with turbulence intensities in the order of 0.2 % [19] (measured in front of the nozzle without the test section attached). A very low inflow turbulence was desired for the present measurements, since it is known that even small fluctuations may have a significant effect on the flow [21].

The flow speed U_∞ inside the test section was controlled by adjusting the pressure inside the settling chamber of the wind tunnel. The correspond-

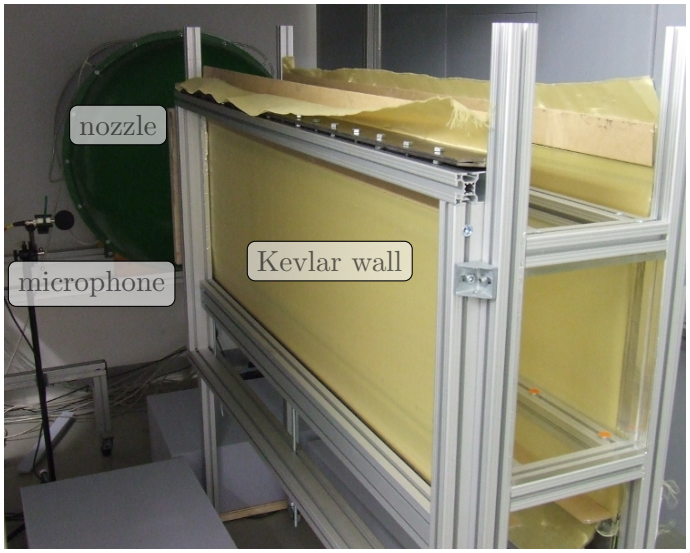

(a) Side view of the test section, showing the setup used for the acoustic measurements

(b) Downstream view, showing the setup used for the measurement of the flap motion

Figure 2: Photographs of the experimental setup in the aeroacoustic wind tunnel

ing flow speeds were determined in a separate measurement using a vane anemometer positioned at the test section exit. The measurement was performed with the reference cylinder in place. To correct for the blockage of the wind tunnel, the simple approximative blockage correction method proposed by Barlow et al. [22] was then applied. Thus, the corrected flow speed U can be derived from the uncorrected flow speed U' as

$$U = U' \cdot \left(1 + \frac{1}{4}\frac{d}{b}\right), \tag{3}$$

where $b = 0.23$ m is the width of the test section.

For the measurements, the cylinders were positioned approximately 0.2 m downstream from the nozzle and centered between the two Kevlar windows. The models were fixed to the acrylic glass walls on both ends, and hence a generation of tip noise did not occur. Additionally, it is known from past studies [23, 24] that a certain two-dimensionality of the flow, for example through the use of end plates, is important and has a noticeable effect on the noise generation.

2.2. Cylinder models

2.2.1. Fabrication of cylinder models with hairy flaps

Previous experimental works have successfully used silicone rubber for manufacturing flap structures [25, 26]. Silicone based materials offer a broad scope for adjusting the material properties, e.g. the Young Modulus can be tuned depending on the mixing ratio of silicon to its curing agent as well as on the curing procedure. Furthermore, the properties of these materials do not change noticeably under temperature differences, which facilitates the reproducibility of experiments.

In the present experimental setup, several flap rows were individually cast as a ring with eight parallel flap structures of silicone rubber Elastosil RT 601, presenting a Young Modulus of 1.2 MPa. This was done using a casting mold, which contains metal plates of two different thicknesses that are alternately placed in order to form small gaps that will become the flaps. The resulting thickness of the flaps is around 0.3 mm, and their length and spacing are 9 mm and 3.6 mm, respectively (see Figure 3). Due to some misalignment of the metal plates and irregularities on their edges, the flap thickness presented a small variability among the flaps, whose influence on the experiments will be further discussed in Section 2.5. The silicone rubber

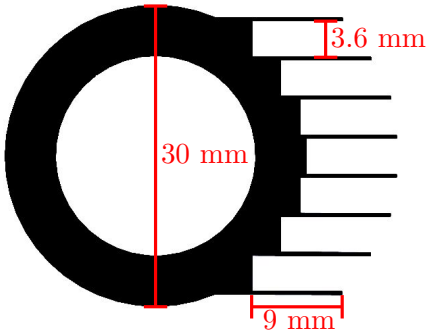

Figure 3: Shape and dimensions of a flap ring segment (the thickness of the flaps is 0.3 mm)

was produced using a mixing ratio equal to 9:1 of silicon to its curing agent. After mixing the two components, the silicone was placed in a vacuum chamber in order to eliminate the presence of small bubbles. This procedure was repeated consecutively after filling the casting mold with additional silicon material in order to ensure that the small gaps between the metal plates were completely filled. After the filling procedure was completed, the curing of the silicone in the molds was carried out under room temperature for about 24 hours. The resulting flap rings have a thickness of 12 mm, and in total 22 flap rings were positioned on a rigid PVC cylinder. Small rings with a thickness of 1 mm were placed between two consecutive flap rings in order to ensure a small gap between neighboring flap rows.

A modal analysis was performed for such a flap ring using a Finite Element method. It revealed that the eigenfrequency of the first bending mode of the flaps is about 22 Hz and that of the first torsional mode is 39 Hz.

2.2.2. Additional cylinder models

Besides the hairy flap cylinder, measurements were also performed on four other cylinder models. This included

- a smooth circular cylinder used as a reference (named "reference"),
- the same smooth circular cylinder, but with additional tripping tape attached (named "reference, tripped"),
- a cylinder with a solid aft body that has the same dimensions as the envelope of the hairy flap cylinder (named "aft body"),

Table 1: Geometrical characteristics of the cylinders used in the present study

cylinder model	**description**
reference	smooth circular cylinder made from polyvinyl chloride
reference, tripped	smooth circular cylinder with tripping tape applied
hairy flaps	cylinder with eight flexible flaps made from silicone rubber
fur	cylinder modified with a 27 mm wide strip of adhesive tape with fur
aft body	cylinder with bluff aft body

Figure 4: Photograph of the cylinders used in the present study (from left to right: reference, aft body, fur and hairy flaps)

- a cylinder that has a wide strip of fur of approximately 27 mm glued to the downstream region (named "fur"), where the length of the single hairs of the fur was about 15 mm.

The tripping tape of the second cylinder had a width of 1 mm and a height of 0.2 mm. Following the approach by Igarashi [14], it was applied at an angle of $\pm 50°$ to the flow over the whole span of the cylinder. The aft body cylinder was considered in order to identify whether the effect connected to the hairy flap cylinder may only be due to its outer shape. Likewise, the cylinder with fur was considered in order to examine whether similar effects as those described by Kunze and Brücker [8] may also occur for other flexible add-ons. An overview of all cylinders examined in the present study is given in Table 1 and a photograph can be seen in Figure 4. Each cylinder has a diameter 0.03 m and a length l of 0.28 m, resulting in an aspect ratio l/d of 9.3. A rather large aspect ratio was desired since it is known that the aspect ratio strongly affects the vortex shedding behavior [27, 28].

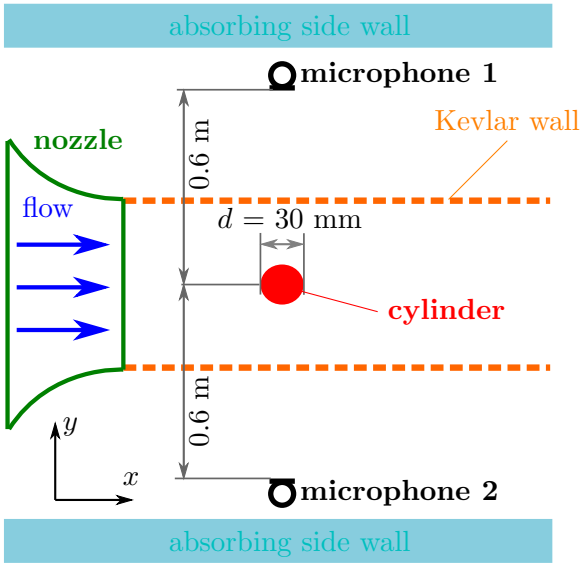

Figure 5: Schematic (top view) of the setup used for the acoustic measurements (not to scale)

For each of the cylinders given in Table 1, measurements were conducted at flow speeds between 7 m/s and 17 m/s, which lead to Reynolds numbers (based on the cylinder diameter) from 14,600 to 34,000 and Mach numbers between 0.02 and 0.05. Therefore, the resulting tonal noise due to vortex shedding can be expected to occur at frequencies between approximately 50 Hz and 100 Hz for the reference cylinder. Additional acoustic measurements were performed without a cylinder in place to characterize the background noise inside the wind tunnel facility.

The resulting range of Reynolds number considered for the present study is known as the subcritical range, which is characterized by a laminar near-wake with vortex street instability [29]. In this regime, transition takes place in the shear layers. According to the study from Wieselsberger [30], above the critical Reynolds number the separation point is shifted towards the rear, which is connected to the fact that the flow "becomes permeated with small vortices" and hence the surface layer becomes turbulent.

2.3. Setup of acoustic measurements

The acoustic measurements were performed using two 1/4th inch free field ICP microphones, which have a sensitivity of 50 mV/Pa. They were

positioned at a distance of 0.6 m from the cylinder axis, perpendicular to the flow on opposite sides of the test section (see Figure 5). To test the reproducibility and to increase the statistical significance of the results, each measurement was performed twice (in completely individual measurement series). For each measurement, the data were recorded over a duration of 90 s with a sampling frequency of 51.2 kHz using a 24 Bit National Instruments digital signal acquisition module NI-USB 4431. The data were then transferred into the frequency domain by applying a Fast Fourier Transformation (FFT). To this end, the sampled signal was divided into blocks with a length of 131,072 samples using a Hanning window. This lead to a frequency spacing of the resulting sound pressure level spectra of 0.39 Hz.

In general, different methods are available to process the measured acoustic data. One method is the direct use of the auto spectral density from one of the microphones. Additionally, the results may be improved by subtracting the wind tunnel background noise. Another possible procedure is the use of the coherent output power method [31] which takes advantage of the fact that the noise measured by microphone 1 and 2, and hence on opposing sides of the cylinder, is coherent when generated by the cylinder. A third method, which makes use of the same fact, is to add the time signals from both microphones with a phase delay of 180°, which is actually equivalent to a subtraction of both signals. Thus, a theoretic dipole behavior is assumed. This approach has the advantage that unwanted noise sources, which may also be measured by both microphones, but which are in phase, will be omitted. For example, these could be reflections of the cylinder generated noise from the bottom or ceiling of the test section. After all three methods were tested on the data, it was decided to use the third method for the present investigation. Finally, the magnitude of the sound pressure levels was corrected by subtracting 6 dB.

2.4. Setup of constant temperature anemometry measurements

In order to obtain a better understanding of the effect of the flaps on the characteristics of the cylinder wake, spectra were measured of the turbulent velocity fluctuations in the shear layer using constant temperature anemometry. Following the method used by Bearman [32], this was done at a single measurement position one cylinder diameter downstream and one half diameter off center from the cylinders approximately at mid-span. In order to allow access for the hot-wire probe, one of the Kevlar walls was

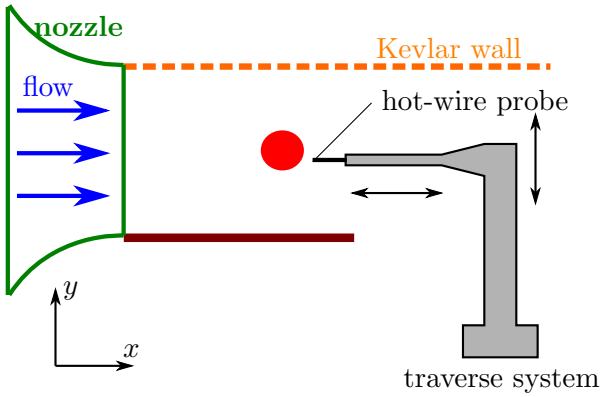

Figure 6: Schematic (top view) of the setup used for the CTA measurements (not to scale)

removed from the test section. To keep the flow at the position of the cylinders two-dimensional, the front part of the open window was covered with a board of 0.3 m length. In this case, the flow velocity was obtained from an additional measurement using a vane anemometer positioned approximately 0.2 m downstream from the reference cylinder. Although the adjusted pressures in the settling chamber were identical to the values used in the acoustic measurements, the absence of one of the Kevlar walls lead to slightly different flow speeds and hence to different Reynolds numbers.

The constant temperature anemometry measurements were conducted using a Dantec P11 type single wire probe and a Dantec multi-channel CTA measurement system. The data were recorded with a sampling frequency of 25.6 kHz using a 24 Bit National Instruments digital signal acquisition module (type NI-USB 4431). A 3D traverse system made by Isel, which has a minimum step size of 0.1 mm, was used to position the probe. Similar to the processing of the acoustic data, a large measurement duration of 80 s was chosen in order to obtain a sufficient statistical significance. The first second of the measured data was later removed in post processing in order to avoid any effects of potential vibrations after each step of the traverse system. The remaining time data were then Fast-Fourier-transformed into the frequency domain, using blocks with a size of 65.536 samples and an overlap of 50 %. This lead to the same frequency spacing for the power spectral density Φ of the turbulence as for the sound pressure level spectra.

2.5. Setup of flap motion measurements

In order to monitor the motion of the flaps, a high speed camera (Phantom V12.1-8 G-M, Vision Research) with a 35 mm Nikon lens was positioned below the wind tunnel with an inclination angle of 45° relative to the axial flow direction, as shown in Figure 2(b). In order to reduce the influence of wall effects promoted by the boundary layers of the wind tunnel, the high speed camera was focused on the flap rows positioned at the midspan of the cylinder. For the purpose of improving the visualization and facilitating the image analysis, the recorded flap rows were painted in the following manner: flap tips with white color and the space between flaps with black color. Additionally, a continuous light source was positioned downstream from the wind tunnel. For all tested cases, the frame rate of the high speed camera was 500 Hz with an exposure time per frame of 500 μs.

The flap motion measurements were only conducted for Reynolds numbers up to 26,000, since at higher Reynolds numbers it occasionally occurred that neighboring flaps collided.

Image sequences, each one recorded during a period of 14 s (corresponding to 7,000 images per sequence according to the frame rate of the camera), were post-processed to obtain the movement of the flap tips. First, each image in the sequence was cropped in order to retain only the center row of flaps. This section was then binarized, and finally the centroid location as well as the trailing-edge tilt angle of each flap tip were measured. Figure 7 shows the comparison between the original image and the respective treated version for a particular instant of time, where the colored dots in the treated image indicate the instantaneous centroid location, calculated for each flap tip. In Section 3.3, results will be discussed for flap number 5, representing an inner flap, and flap number 8, representing an outer flap.

Based on the recorded time series of the centroid coordinates of the flaps, the frequency spectrum of the flap tip movement can be calculated for each flap in the x- and y-directions. Due to the limited number of time samples, the spectrum was not obtained by an FFT, but rather by an autoregressive (AR) model. In this case, a Burg algorithm [33] with an order of 42 was applied to the measured time data in order to obtain the corresponding power spectral densities.

2.6. Setup of flow visualization measurements

In order to obtain more information about the wake behavior of the cylinder models, additional experiments were conducted with fog visualization in

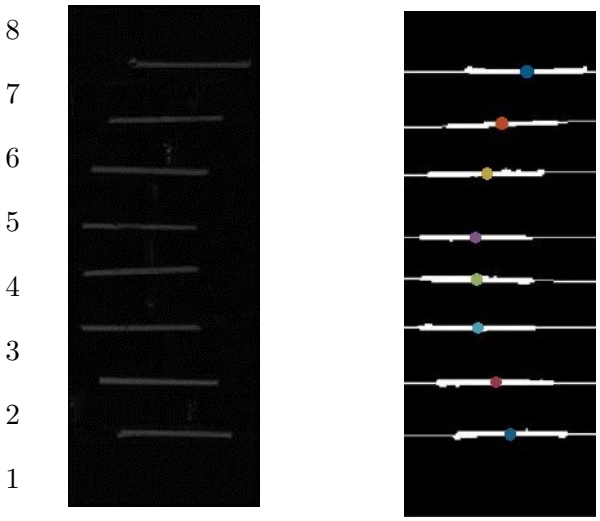

(a) Original image (b) Treated image

Figure 7: Original image and respective treated image of the selected flap row obtained after post-processing (colored dots and thin white lines on the treated image indicate the calculated centroid location and inclination of each flap; flap motion along vertical axis, cylinder axis corresponds to horizontal axis)

the wind tunnel of the Institute of Mechanics and Fluiddynamics at the TU Bergakademie Freiberg. The open measurement section has a cross-sectional area of 0.4 m × 0.5 m. As with the aeroacoustic wind tunnel, turbulence intensities in this facility are very low (< 0.2 %). For the visualization, a pressure vessel was filled with oily fog fluid at 1 bar and, attached to the bottom of the vessel, a flexible tube drove the fluid towards a thin a metal tube of 1 mm in diameter, which was heated in order to create the fog. This metal tube was positioned in the middle of the measurement section 0.3 m upstream from the cylinder.

The experiments were carried out with the untripped reference cylinder and the hairy flap cylinder. In order to ensure a good consistency with the measurements performed in the aeroacoustic wind tunnel (see Section 2.1), end plates were attached to the cylinder ends. Below the setup, a continuous laser (4 W, Dantec Ray Power 2000) created a 2-3 mm thick laser sheet in streamwise direction. Due to the presence of the end plates that limited the vision access to the cylinder, the high speed camera was not aligned perpendicular to the laser sheet, but was rather positioned at an angle of about 30° and recorded with a frame rate of 400 Hz at an exposure time of 1.1 ms. Image sequences of 600 frames were then superposed into one image in order to obtain a clearer picture. Thus, the resulting images show a time-averaged distribution of smoke in the wake of the cylinders, which gives a qualitative impression of the extent of the separation bubble and shear layers.

3. Experimental Results

In this section, the results from the acoustic measurements, the constant temperature anemometry measurements, the flap motion measurements and the flow visualization measurements will be presented and discussed.

3.1. Results of the acoustic measurements

As a first step, the overall noise generated by the different cylinders presented in Table 1 will be compared. Figure 8 shows the measured sound pressure levels determined from the phase-corrected addition of the signals from microphone 1 and microphone 2. Only the results from one measurement are shown for each Reynolds number and each cylinder. The background noise data shown in Figure 8 correspond to the auto spectra of microphone 1 for measurements with an empty test section.

It is visible that all three cylinder modifications (hairy flaps, fur and aft body) have a noticeable effect on both the broadband noise, which is especially visible at medium and high frequencies above 1 kHz, as well as on the vortex shedding tone, as the amplitude and center frequency of the main tonal peak are different from that of the untripped reference cylinder. The exact effect of the modifications on the frequency of the vortex shedding noise (the aeolian tone), which is of main interest in the present study, will be examined in more detail in the remainder of this section. Still, it can already be concluded from the sound pressure levels shown in Figure 8 that all modifications lead to a noticeable decrease of the peak amplitude and a shift of the peak frequency. In more or less all cases, the amplitude of the harmonics is nearly completely suppressed. However, it also becomes visible from Figure 8 that some of the modifications lead to an increase of the broadband noise compared to the untripped reference cylinder, mainly at higher frequencies.

The sound pressure level spectra from the untripped reference cylinder are characterized by three tonal peaks, which, depending on the Reynolds number, correspond to the vortex shedding noise and its first harmonics. This overall spectral shape is in good agreement with the results reported in other studies [34]. Even at the lowest Reynolds number of 14,600, the broadband noise generated by the reference cylinder significantly exceeds the wind tunnel background noise for frequencies up to approximately 300 Hz. At the highest Reynolds number of 34,000, the broadband noise of the reference cylinder is up to 10 dB above the wind tunnel background noise for frequencies up to 1 kHz. The light tripping of the reference cylinder has no notable influence on the measure sound pressure levels. At Reynolds numbers of 18,900 through 23,300, the tonal peak due to vortex shedding seems to be shifted to slightly higher frequencies, indicating that the tripping tape merely corresponds to a small increase of the effective cylinder diameter in this Reynolds number range.

It can be observed that there exists a strong narrow peak of the wind tunnel background noise at a frequency of 100 Hz. Since the frequency of this peak is independent of the Reynolds number, it is not an aeroacoustic source, but most likely electrical noise generated by the wind tunnel power unit. This peak exceeds the measured spectra from the cylinders in the lower Reynolds number cases. However, it does not affect the vortex shedding noise peak.

The sudden shift of the vortex shedding peak due to the existence of

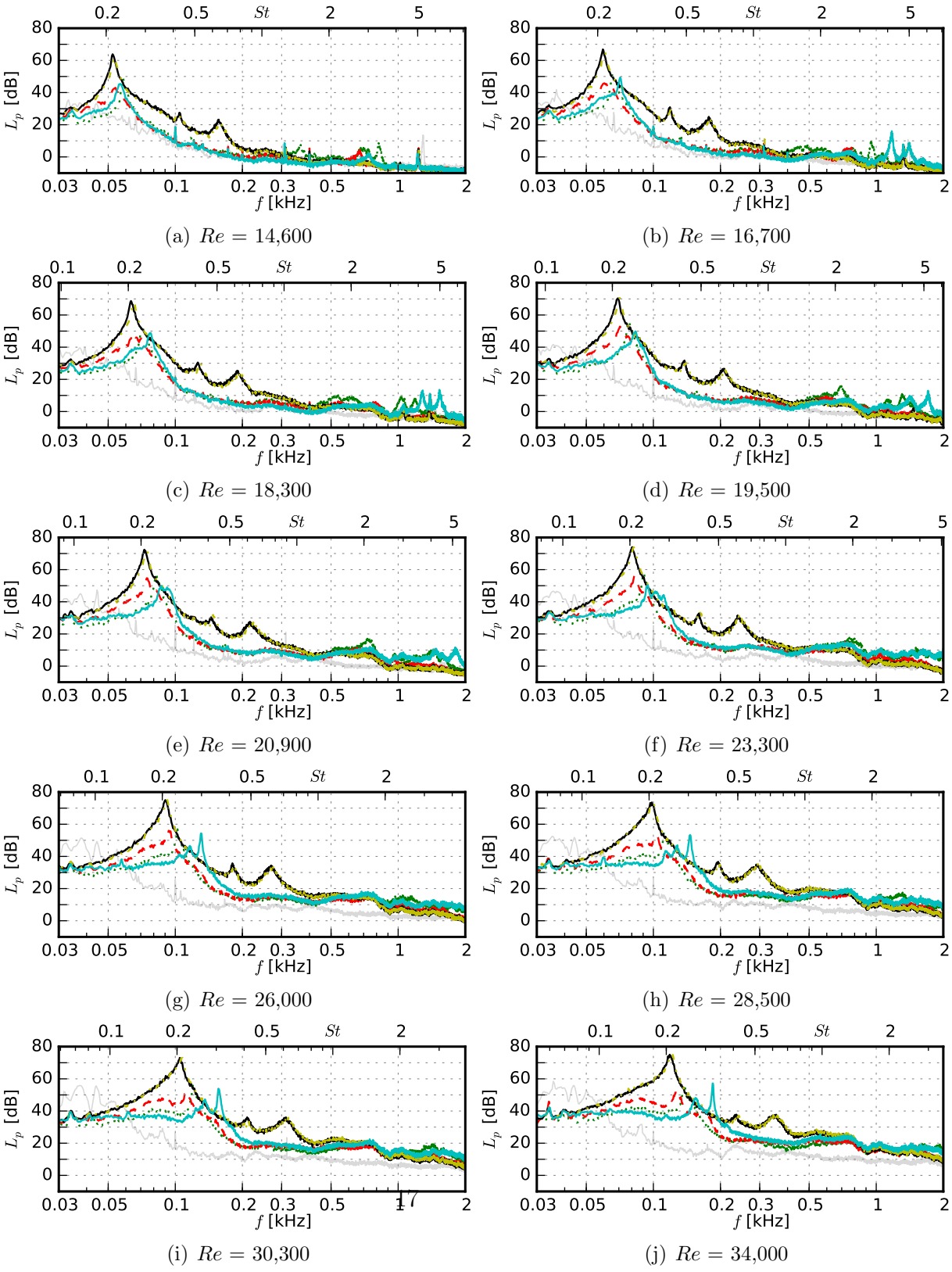

(a) $Re = 14{,}600$ (b) $Re = 16{,}700$

(c) $Re = 18{,}300$ (d) $Re = 19{,}500$

(e) $Re = 20{,}900$ (f) $Re = 23{,}300$

(g) $Re = 26{,}000$ (h) $Re = 28{,}500$

(i) $Re = 30{,}300$ (j) $Re = 34{,}000$

Figure 8: Sound pressure level spectra *re* $2{\cdot}10^{-5}$ Pa of all cylinders from Table 1 (▬ reference, ▬● reference, tripped, ▬ hairy flaps, ●●● fur, ▬▬ aft body, ▬ background noise)

the flaps, as described by Kunze and Brücker [8], can be seen very clearly in the sound pressure levels obtained for the hairy flap cylinder. At the lowest Reynolds number, the spectral peak is close to the peaks observed for the other cylinders, while with increasing frequency this peak shifts toward higher Strouhal numbers. It is visible that this shift does not occur quite so suddenly, but rather gradually, which happens approximately between $Re = 19{,}500$ and $Re = 26{,}000$. In this range, the spectra consist of a broad hump with a relatively narrow maximum on top. With increasing Reynolds number, the hump shifts to higher frequencies, while first a second maximum (at $Re = 26{,}000$) and, finally, a third maximum ($Re = 28{,}500$) develop at frequencies below that of the main maximum. These additional peaks are lower in level than the main peak. The existence of these secondary maxima hints at some kind of bifurcation process, although no detailed hypothesis can be made based on the present data.

Interestingly, the spectra generated by the hairy flap cylinder do not show distinct harmonics of the vortex shedding noise of the cylinder as can be found in the spectra of the reference cylinder. At Reynolds numbers from 16,700 to 20,900, the spectra of the hairy flaps show a notable increase of noise at frequencies above 1 kHz, visible as several sharp spectral peaks. This increase in noise has to be caused by the presence of the flaps, but based only on the acoustic results the exact reason is not clear. It may be related to the motion of the flaps or even some kind of flap vibration. It is also possible that this increase is a contribution of self noise from the flaps, which may include noise generated by the interaction of the boundary layer along the flaps with the flap trailing edge as well as a sort of flap trailing edge bluntness noise. At Reynolds numbers above 20,900, no such peaks are visible any more.

For frequencies approximately up to 500 Hz, the noise generated by the cylinder with the fur modification is below that from the reference cylinder with the exception of several small peaks that are visible especially at low Reynolds numbers. At $Re = 14{,}600$, these peaks are visible around 350 Hz and between 650 Hz and 900 Hz. With increasing Reynolds number, the first peak becomes broader, turning into a small hump whose frequency range increases with further increasing Reynolds number. The peaks between 650 Hz and 900 Hz are also shifted towards higher frequencies, but remain sharp. It is reasonable to assume that these effects are due to some vortex shedding at the small, forward facing step on each side of the cylinder, produced by the adhesive tape that holds the fur. At Reynolds numbers of 23,300 and above, no additional peaks are visible and the broadband noise spectral shape of

the fur cylinder resembles that of the reference cylinder. Apart from the described increases in flow noise, the fur is responsible for the complete suppression of the first and second harmonics of the aeolian tone. This is in good agreement with the results of Nishimura et al. [16], who performed measurements on cylinders covered by pile fabrics and found a noticeable decrease of the vortex shedding peak. The aft body modification also helps with suppressing the harmonics of the vortex shedding noise. In general, it has only a small effect on the broadband noise generation in the frequency range above the harmonics. With the exception of a narrow noise increase between approximately 600 Hz and 700 Hz at Re = 14,600 and between 700 Hz and 800 Hz at Re = 16,700, the aft body modification is the only one that does not lead to a strong increase of noise at medium and higher frequencies.

As could already be concluded from the spectra shown in Figure 8, the hairy flaps as well as the other modifications have a noticeable effect on the aeolian tone. The influence of the hairy flaps on the location of the vortex shedding tone is very special, as a shift of the peak frequency seems to appear. To further examine this phenomenon, Figure 9 shows the corresponding Strouhal number of the vortex shedding tone. Thereby, the Strouhal number was calculated using the frequency corresponding to the maximum sound pressure level, and hence the highest peak, in the acoustic spectra. Since each measurement was performed twice, the peak Strouhal number St shown Figure 9 is the average value from both peak Strouhal numbers.

The Strouhal number determined for the reference cylinder remains nearly constant at approximately 0.21, which is in good agreement with the theoretical value in this Reynolds number range [29]. The values obtained for the tripped reference are slightly above those of the untripped reference. This indicates that the transition of the boundary layer has no grave effect on the shedding frequency.

The shift of the vortex shedding Strouhal number obtained for the hairy flap cylinder can now be seen even more clearly. While Figure 8 showed that the shift already starts around a Reynolds number of 20,000, the Strouhal number associated with the highest peak in the spectra remains nearly constant with a value around 0.25 at Reynolds numbers up to approximately 23,300. The Strouhal number Re = 23,300 is lower than the remaining values in this range. This is due to the fact that at this Reynolds number the selected peak is only the first one of three maxima that are visible, situated on the left side of the broader hump. This maximum at f = 94 Hz is only

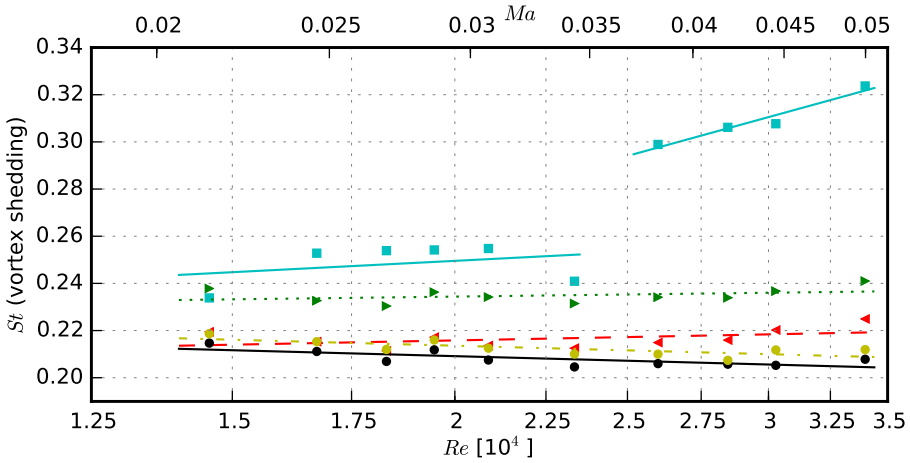

Figure 9: Dependence of the peak Strouhal number St obtained from the acoustic measurements on the Reynolds number Re for the cylinders, the line represents a linear approximation of the measured data (● reference cylinder, ● reference, tripped, ■ hairy flaps, ▶ fur, ◀ aft body)

insignificantly higher than the second maximum at $f = 101$ Hz, which would lead to a Strouhal number just below 0.26. In the Reynolds number range from 23,300 to 26,000, the Strouhal number increases drastically to values in the order of 0.30. This corresponds to the shift of the vortex shedding peak that is visible in Figure 8, where the first small maximum (at 94 Hz) suddenly jumps to a frequency of 131 Hz. At Reynolds numbers above 26,000, the Strouhal number remains very high and increases slightly from about 0.30 to 0.32. The observation of the sudden increase of the Strouhal number of the vortex shedding noise is in agreement with the alteration of the natural vortex separation cycle by the hairy flaps as described by Kunze and Brücker [8]. The only difference is that the Reynolds number, at which the shift was observed, is different. While it was about 14,000 in the experiments by Kunze and Brücker, it takes a value of approximately 19,500 to 26,000 in the present study. This difference is due to the fact that the experiments in [8] were conducted in a water tunnel, where the added mass effect leads to a different behavior of the flap motion. The added mass effect basically describes the increase of the inertia of the moving flaps due to the fact that the volume of the surrounding fluid has to be accelerated as well [35]. The fact that neither the cylinder modified with the strip of fur nor the aft body cylinder show at least a similar effect indicates that the jump of the vortex

shedding Strouhal number has to be caused by the properties and configuration of the flaps, thus following the argumentation from Kunze and Brücker. Based on the acoustic results alone it is not clear how exactly the flaps alter the vortex shedding. It is reasonable to assume that such a jump in the *St*-*Re*-relation will also be visible in the measured spectra of the velocity fluctuations in the shear layer.

The Strouhal numbers of the tonal noise generated by the fur cylinder and the aft body cylinder are approximately constant over the whole range of flow speeds. For the fur cylinder, it takes a value of just below 0.24, which is higher than that of the reference cylinder. This may be caused by the fact that the strip of fur leads to a virtual increase of the cylinder diameter. The Strouhal number associated with the aft body cylinder takes a value of approximately 0.22, and hence is only slightly above that of the reference cylinder.

3.2. Results of the constant temperature anemometry measurements

The spectra of the turbulent velocity fluctuations Φ, measured in the shear layer of the cylinders, are given in Figure 10. The plots basically support the findings from the acoustic measurements shown in Figure 8: At Reynolds numbers below 23,800, the peak obtained for the flap cylinder is only slightly above that of the reference cylinder. At $Re = 23{,}800$, the peak is more or less abruptly shifted to a higher frequency. At further increasing Reynolds numbers, the peak remains at this higher Strouhal number. At the highest Reynolds number of 25,500, it can also be seen that the broadband values obtained for the flap cylinder are below that of the other cylinders. This is due to the fact that, as shown in Figure 1, the main effect of the flaps is to shift the vortices from the Kármán vortex-street towards the centerline, an effect that increases with increasing flow speed. Hence, at the highest Reynolds number of the CTA measurements the hot-wire probe was simply not located in the center of the shear layer any more, resulting in an overall decrease of the turbulent kinetic energy.

As in the acoustic spectra, all modified cylinders do not feature any harmonic of the vortex shedding peak, which is only visible for the reference cylinder. An interesting feature can be seen in Figure 10: Only the spectra measured in the shear layer of the fur cylinder show an increase of the turbulent velocity fluctuations at higher frequencies (for example around 800 Hz at $Re = 13{,}500$ and around 1 kHz at $Re = 17{,}200$). A similar peak has been observed in the acoustic spectra (see Figure 8). The other modified cylinders

do not show any additional spectral increase. Thus, the remaining narrow band features observed in the acoustic spectra at frequencies above the aeolian tone do not have their counterpart in the velocity fluctuations within this part of the shear layer. However, it has to be noted that the constant temperature measurements were performed at one span-wise position only. For the flap cylinder, this means the measurement took place in the wake of one single flap ring only, while the measured noise was generated by all 22 flap rings. It is therefore reasonable to assume that some of the acoustic narrowband features are related to velocity fluctuations that occur at other span-wise positions.

In the study of Bearman [32] it was found that the vortex shedding peak becomes much broader when transition to the supercritical regime occurs, which would also be associated with a jump in the Strouhal number towards higher values. Bearman suggests "that the disappearance of narrow-band vortex shedding could be taken as a criterion for determining the end of the critical regime". Since no noticeable broadening of the vortex shedding peak of the flap cylinder can be seen in Figure 10, it does not seem likely that the effect of the flexible flaps is to promote transition to the supercritical regime.

Similar to the analysis of the acoustic spectra, the Strouhal numbers due to vortex shedding were extracted from the spectra shown in Figure 10 and are given as a function of Reynolds number in Figure 11. To enable a direct comparison with the *St*-*Re*-relation for the flap cylinder obtained from the acoustic measurements, the corresponding data from Figure 9 are also included. It is visible that in the constant temperature anemometry data, the jump of the Strouhal numbers seems to occur at a lower Reynolds number. Still, this could again be related to the fact that these measurements were conducted at a single span-wise position only. There is, however, satisfying agreement regarding the absolute value of the Strouhal number. It takes values around 0.25 in the lower range of Reynolds numbers and then jumps to values of 0.28 and 0.3. It can be concluded that, in general, the findings from the velocity fluctuation measurements in the shear layer support the observations from the acoustic measurements, although no additional insight was gained regarding the cause of the sudden jump of the Strouhal number for the flap cylinder.

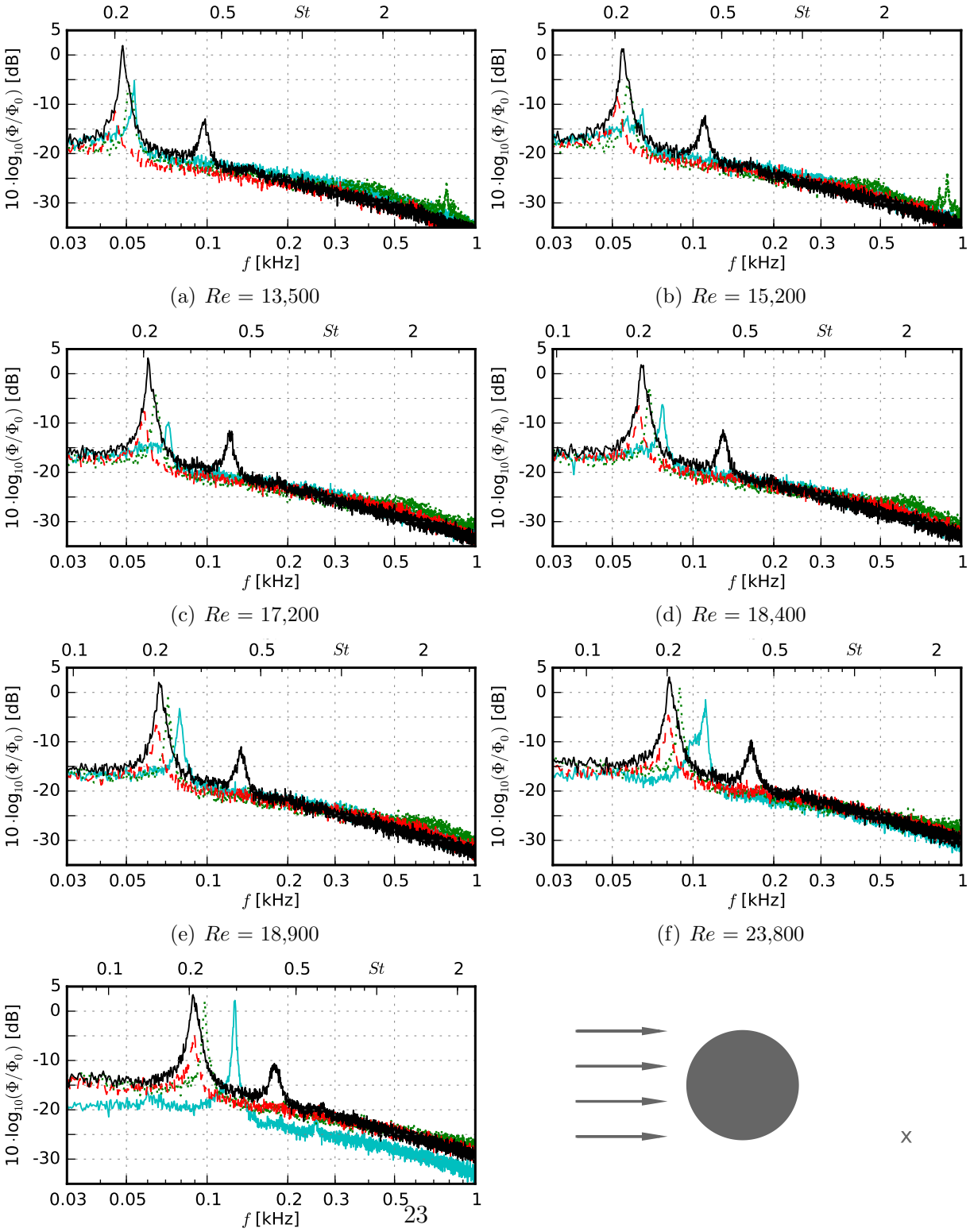

(a) $Re = 13{,}500$

(b) $Re = 15{,}200$

(c) $Re = 17{,}200$

(d) $Re = 18{,}400$

(e) $Re = 18{,}900$

(f) $Re = 23{,}800$

(g) $Re = 25{,}500$

(h) position of the hot-wire probe (marked by the '×')

Figure 10: Spectra of the turbulent velocity fluctuations of all cylinders from Table 1, non-dimensionalized with $\Phi_0 = 1$ m^{2}s^{-1}, ▬ reference, ▬ hairy flaps, ••• fur, ▬ ▬ aft body

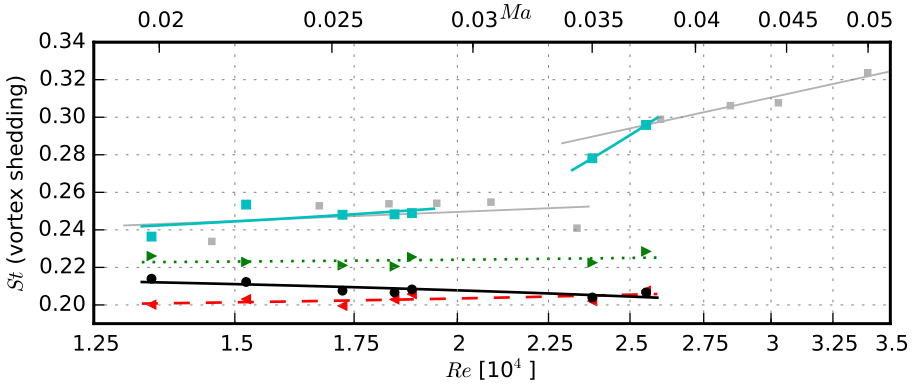

Figure 11: Dependence of the peak Strouhal number St obtained from the hot-wire measurements on the Reynolds number Re for the cylinders (● reference cylinder, ■ hairy flaps, ▶ fur, ◀ aft body, ▪ hairy flaps, acoustic)

3.3. Results of the flap motion measurements

Results of the flap motion measurements for one inner flap (flap number 5) and one outer flap (flap number 8) are displayed in Figure 12 for different Reynolds numbers. Basically, four distinct maxima are visible for each flap. The peak at the lowest frequency is due to the resonance of the single flap. For the inner flap (Figure 12(a)), the resonance appears at a frequency of about 20 Hz, which is close to the frequency of 22 Hz obtained numerically for the first bending mode of the flaps. For the outer flap (Figure 12(b)), the first peak is located between the eigenfrequencies of the first bending mode and the first torsional mode (at $f = 39$ Hz). This behavior can also be observed in the high speed camera movies, which show that the movement of the outer flaps is a combination of oscillatory bending and torsion, while the inner flaps rather perform an exclusive bending motion. This seems reasonable when it is kept in mind that the outer flaps directly interact with the shear layer. In a frequency range between 50 Hz and 100 Hz, the spectra feature a second peak, the frequency of which increases with increasing Reynolds number. It corresponds to the vortex shedding at the flap cylinder. At higher frequencies, the spectra feature two additional peaks which are resonances of the flap ring, which constitutes an oscillating system composed of the eight flaps and the fluid between them. The amplitude of the first resonance peak (denoted "resonance A") increases with increasing Reynolds number. At the highest Reynolds number of 26,000, the flap motion spectra of the inner flap do not show two separate peaks for the vortex shedding and

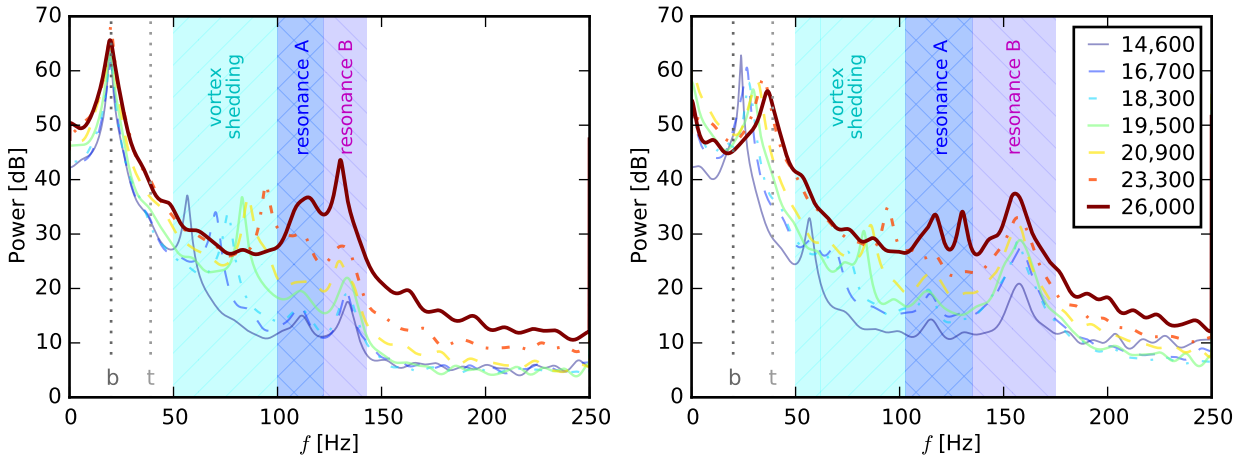

(a) Results obtained for inner flap (flap 5)

(b) Results obtained for outer flap (flap 8)

Figure 12: Spectra obtained for the movement of one inner flap and one outer flap using a Burg algorithm [33] for different Reynolds numbers (dotted gray lines represent the eigenfrequencies of the first bending mode, b, and the first torsional mode, t, of the single flaps)

resonance A, but only one broader peak. The second resonance ("resonance B") is visible at a fixed frequency of about 130 Hz for the inner flap and around 157 Hz for the outer flap (for the second outer flap the peak appears around 170 Hz). The amplitude of this peak strongly increases with increasing Reynolds number, and overall it is much higher for the outer flap than for the inner flap. Interestingly, at a frequency of 130 Hz (which corresponds to the center frequency of this peak for the inner flap) the acoustic spectra shown in Figure 8 featured a narrow, sharp maximum for Reynolds number above 23,300.

Due to the fact that the flap motion spectra contain several distinct maxima, the most obvious cause of the jump of the Strouhal number described by Kunze and Brücker [8] is a lock-in effect between the vortex shedding peak and the resonances of the flap ring. This is visible in Figure 12(a) at the highest Reynolds number, where the vortex shedding peak and resonance A of the inner flap are merged (note that this merging did not yet occur for the outer flap, showing that, at least to a certain degree, the flaps oscillate individually). To further examine this effect, the two resonances (A and B) found in the flap motion spectra are used to calculate corresponding Strouhal

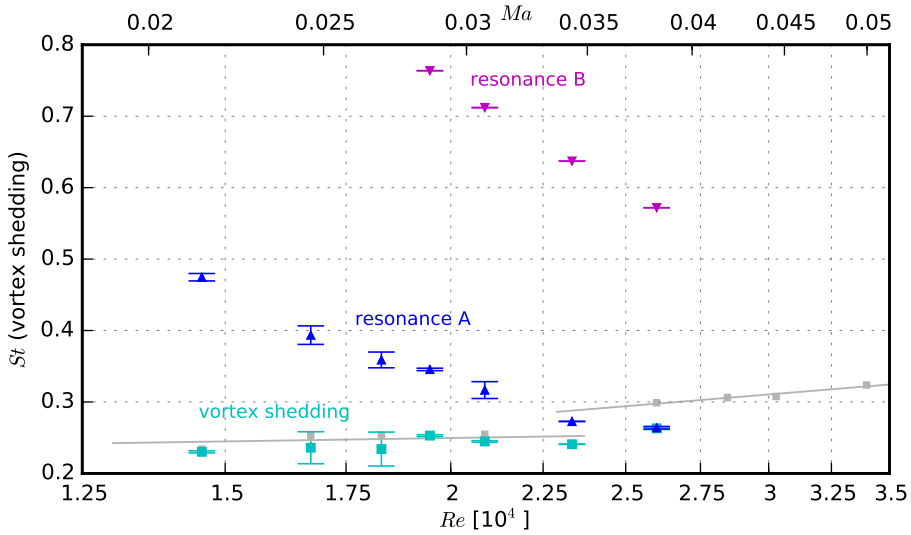

Figure 13: Dependence of the peak Strouhal number on the Reynolds number for the hairy flaps, ■ data obtained from the vortex shedding peaks of all eight flaps, ▲ data obtained from the first resonance peak, A, of the two outer flaps, ▼ data obtained from the second resonance peak, B, of the two outer flaps (see Figure 12), ▪ hairy flaps, acoustic (data contain measured standard deviation)

numbers. The resulting vortex shedding Strouhal number was obtained as the average over the corresponding Strouhal numbers from all eight flaps of the selected flapring. The Strouhal numbers belonging to the two resonances were obtained as the average of the data from the two outer flaps only, since differences between single flaps were larger for these peaks than for the vortex shedding peaks. Additionally, it can be assumed that the outer flaps contribute more strongly to the jump of the Strouhal number. The resultant St are shown in Figure 13 as a function of the Reynolds number. For a better comparison, the peaks obtained for the hairy flap cylinder from the acoustic measurements (Figure 9) are also included.

It is visible that the Strouhal numbers derived from the vortex shedding peaks in the flap motion spectra basically show the same dependence on the Reynolds number as those obtained from the acoustic measurements in the lower range of Reynolds numbers. Regarding the cause of the Strouhal number jump, which occurs between Re = 23,300 and 26,000, Figure 13 shows that the jump is caused by a lock-in of the vortex shedding frequency with the first resonance of the flap ring visible in the spectra in Figure 12.

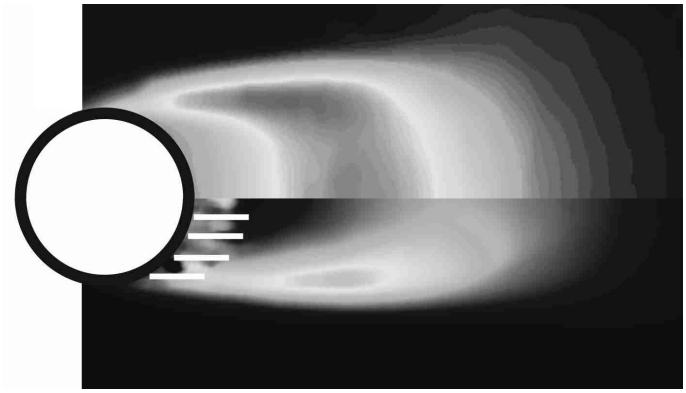

Figure 14: Time-averaged wake structure of a plain cylinder (top) and a cylinder with hairy flaps (bottom) at Re = 24,900 (averaging time 1.1 ms, gray scales represent regions of approximately constant smoke concentration)

The Strouhal numbers that would be related to the second resonance are too high, making a lock-in with this peak rather unlikely in this Reynolds number range.

3.4. Results of the flow visualization measurements

Figure 14 shows the results from the flow visualization experiments for the untripped reference cylinder and the hairy flap cylinder at a Reynolds number of 24,900. Longitudinal structures are visible in the streamwise direction on the upper and lower part in the wake, which correspond to the shear layers formed between the outer flow and the separation bubble. The transversal spacing between these shear-layers is a rough representation of the width of the separation bubble. The images show that the flexible flaps lead to a more slender separation bubble compared to the reference cylinder. Hence, the flow visualization measurements confirm the findings from Kunze and Brücker as summarized Figure 1.

4. Conclusions

In a recent study by Kunze and Brücker [8] it was observed that hairy flaps attached to the aft end of a circular cylinder lead to a characteristic jump in the Strouhal-Reynolds number relation as a consequence of a lock-in between the eigenfrequency of the flaps or the bundle of flaps and the vortex shedding frequency. Motivated by that work, the research described

in the present paper is focused on the vortex shedding noise generated by such a hairy flap cylinder. To this end, acoustic measurements and hot-wire anemometry measurements were performed in an aeroacoustic open jet wind tunnel, while the motion of the flaps was captured simultaneous using a high speed camera. Additionally, flow visualization measurements were conducted in order to obtain qualitative information on the extent of the separation bubble behind the cylinder. Besides the hairy flaps, a set of other cylinder modifications was examined.

The results from the acoustic measurements showed that the jump in the Strouhal-Reynolds relation is also visible in the acoustic spectrum in case of the hairy flaps while neither of the other modifications replicates this behavior. This was also confirmed by the spectra of the turbulent velocity fluctuations measured in the shear layer. This is in good agreement with the results from Kunze and Brücker. However, the specific Reynolds number where the jump occurs is lower, in a range between approximately 20,000 and 26,000, which differs from the specific Reynolds number of 14,000 found in [8]. This difference can be attributed to the fact that the former experiments were performed in a water tunnel, where the moving flaps additionally have to accelerate the volume of the surrounding water (added mass). Consequently, the eigenfrequency of the flaps in water is considerably lower than the ones in air. Wake visualization on the hairy flap cylinder and the plain reference cylinder at comparable Reynolds numbers confirmed that with the hairy flaps the wake width is decreased, leading to a more slender separation bubble. Again, this is in good agreement with the findings from Kunze and Brücker who observed that along the jump the shedding cycle changes from a zig-zag pattern to a row of vortices of alternating sign. So the mean separation bubble is smaller in the transversal direction making the wake more slender. The spectral analysis of the flap motion in the present study revealed that the flaps are subject to different oscillations: the major peak found in the spectrum is at around 20 Hz, representing the eigenfrequency of the bending mode (in air) of the flaps seen at all Reynolds numbers. A second peak in the flap motion is observed at a frequency that increases with increasing Reynolds number. This peak is related to the vortex shedding at the cylinder. Two additional resonance peaks are visible within the examined range of frequencies, which are independent of the Reynolds number. It is assumed that these are resonances of the flap system as a whole, which represents a coupled oscillator. In total, the resulting flap motion is a superposition of these different oscillations.

From the analysis of the acoustic spectra, the turbulence spectra and the flap motion spectra, the following conclusion can be drawn: It appears that at low flow speeds, resulting in Reynolds numbers roughly below 20,000, the amplitude of the oscillation is not strong enough to change the shedding cycle. Thus, the vortex shedding is not influenced much by the weak motion of the hairy flaps. With increasing flow velocity, the vortex shedding peak shifts to higher frequencies while at the same time oscillation amplitudes of the flaps increase. Finally, around $Re = 20{,}000$, the shedding frequency reaches the resonance frequency of the coupled oscillator and a lock-in happens. As a result, the vortex shedding Strouhal number jumps (or rather gradually shifts) towards a higher value of around 0.3.

Besides the characteristic jump of the Strouhal number that could be confirmed in the present study, the experiments revealed that the hairy flaps enable a noticeable reduction of both vortex shedding noise as well as broadband noise compared to the reference cylinder. A similar trend is observed for the other modification. Therefore, these wake-manipulators could be applied in aerodynamic systems for noise reduction. The cylinder with flaps also modifies the wake and, as a result, the separation bubble appears more slender.

Acknowledgments

This work was partly funded within the framework of PEL-SKIN project EU-FP7, GA no. 334954. All funding provided and the support of BAE SYSTEMS Sir Richard Olver Chair are gratefully acknowledged. The authors thank Philipp M. Hall for his help with the measurements.

References

[1] E. G. Richardson, Aeolian tones, Proceedings of the Physical Society of London 36 (1) (1923) 153.

[2] O. M. Phillips, The intensity of Aeolian tones, Journal of Fluid Mechanics 1 (06) (1956) 607–624.

[3] B. Etkin, G. K. Korbacher, R. T. Keefe, Acoustic radiation from a stationary cylinder in a fluid stream (aeolian tones), The Journal of the Acoustical Society of America 29 (1) (1957) 30–36.

[4] R. D. Blevins, Review of sound induced by vortex shedding from cylinders, Journal of Sound and Vibration 92 (4) (1984) 455–470.

[5] V. Strouhal, Ueber eine besondere Art der Tonerregung [On an unusual sort of sound excitation], Annalen der Physik 241 ((10)) (1878) 216–251.

[6] A. Roshko, On the wake and drag of bluff bodies, Journal of the Aeronautical Sciences (2012).

[7] K. Kiyoung, H. Choi, Control of laminar vortex shedding behind a circular cylinder using splitter plates, Physics of Fluids 8 (2) (1996), 479–486.

[8] S. Kunze, C. Brücker, Control of vortex shedding on a circular cylinder using self-adaptive hairy-flaps, Comptes Rendus Mécanique 340 (1) (2012) 41–56.

[9] M. M. Zdravkovich, Review and classification of various aerodynamic and hydrodynamic means for suppressing vortex shedding. Journal of Wind Engineering and Industrial Aerodynamics, 7 (2) (1981) 145 – 189.

[10] H. C. Lim, S. J. Lee, Flow control of a circular cylinder with O-rings. Fluid Dynamics Research, 35 (2) (2004) 107-122.

[11] N. W. M. Ko, Y. C. Leung, J. J. J. Chen, Flow past V-groove circular cylinders. AIAA journal, 25 (6) (1987) 806–811.

[12] H. C. Lim, S. J. Lee, Flow control of circular cylinders with longitudinal grooved surfaces, AIAA journal, 40 (10) (2002) 2027–2036.

[13] S. Huang, VIV suppression of a two-degree-of-freedom circular cylinder and drag reduction of a fixed circular cylinder by the use of helical grooves, Journal of Fluids and Structures, 27 (7) (2011) 1124–1133.

[14] T. Igarashi, Effect of tripping wires on the flow around a circular cylinder normal to an airstream. Bulletin of JSME, 29 (255) (1986) 2917–2924.

[15] S. J. Lee, H. C. Lim, M. Han, S. S. Lee, Flow control of circular cylinder with a V-grooved micro-riblet film, Fluid dynamics research, 37 (4) (2005) 246–266.

[16] M. Nishimura, T. Kudo, M. Nishioka, Aerodynamic noise reducing techniques by using pile-fabrics. (1999), 5th AIAA/CEAS Aeroacoustics Conference, AIAA-Paper 99-1847.

[17] J. Vad, G. Koscó, M. Gutermuth, Z. Kasza, T. Tábi, Csörgő, Study of the aero–acoustic and aerodynamic effects of soft coating upon airfoil, JSME International Journal, Series C 49 (3) (2006) 648–656.

[18] E. Sarradj, C. Fritzsche, T. F. Geyer, J. Giesler, Acoustic and aerodynamic design and characterization of a small-scale aeroacoustic wind tunnel, Applied Acoustics 70 (2009) 1073–1080.

[19] T. F. Geyer, E. Sarradj, Circular cylinders with soft porous cover for flow noise reduction, Experiments in Fluids, 57 (30) (2016) 1–16.

[20] T. Morel, Comprehensive design of axisymmetric wind tunnel contractions, Journal of Fluids Engineering, 97 (2) (1975) 225–233

[21] P. W. Bearman, T. Morel, Effect of free stream turbulence on the flow around bluff bodies. Progress in aerospace sciences, 20 (2) (1983) 97–123.

[22] J. B. Barlow, W. H. Rae, A. Pope, Low-speed wind tunnel testing. Third edition., John Wiley & Sons, 1999.

[23] R. T. Keefe, Investigation of the fluctuating forces acting on a stationary circular cylinder in a subsonic stream and of the associated sound field, The Journal of the Acoustical Society of America 34 (11) (1962) 1711–1714.

[24] M. M. Zdravkovich, Flow around Circular Cylinders: Vol. 2: Applications, Oxford University Press, Oxford, 2003.

[25] C. Brücker, D. Bauer, H. Chaves, Dynamic response of micro-pillar sensors measuring fluctuating wall-shear-stress, Experiments in Fluids, 42 (2007) 737–749.

[26] C. Brücker, Interaction of flexible surface hairs with near-wall turbulence, Journal of Physics: Condensed Matter, 23 (18), 184120 (2011)

[27] D. J. Moreau, C. J. Doolan, Flow-induced sound of wall-mounted finite length cylinders, AIAA Journal, 51 (10) (2013) 2493–2502

[28] R. Porteous, R., D. J. Moreau, C. J. Doolan, A review of flow-induced noise from finite wall-mounted cylinders, Journal of Fluids and Structures, 51 (2014) 240–254

[29] H. Schlichting, K. Gersten, Boundary-layer theory (9th edition), Springer Verlag Berlin Heidelberg, 1997.

[30] C. V. Wieselsberger, Neuere Feststellungen über die Gesetze des Flüssigkeits- und Luftwiderstandes [New conclusions on the laws of fluid- and air resistance], Physikalische Zeitschrift, 22 (11) (1921) 321–328.

[31] J. S. Bendat, A. G. Piersol, Random data: analysis and measurement procedures (Third edition), John Wiley & Sons, 2000.

[32] P. W. Bearman, On vortex shedding from a circular cylinder in the critical Reynolds number regime, Journal of Fluid Mechanics, 37 (03) (1969) 577–585.

[33] P. Stoica, R. Moses, Introduction to Spectral Analysis, Prentice-Hall, Upper Saddle River, NJ, 1997.

[34] F. V. Hutcheson, T. F. Brooks, Noise radiation from single and multiple rod configurations, International Journal of Aeroacoustics 11 (3) (2012) 291– 334.

[35] G. G. Stokes, On the effect of the internal friction of fluids on the motion of pendulums, Transactions of the Cambridge Philosophical Society 9 (1851) 8–106.